Carbon 00 (2018) 1–38

Predicting the performance of carbon flow-electrodes for desalination applications via electrochemical impedance spectroscopy

Alexandra Rommerskirchen[a,b], Anna Kalde[a,b], Christian J. Linnartz[a,b], Leon Bongers[b], Georg Linz[a,b], Matthias Wessling[a,b,*]

[a] *DWI - Leibniz Institute for Interactive Materials e.V., Forckenbeckstraße 50, 52074 Aachen, Germany*

[b] *RWTH Aachen University, Aachener Verfahrenstechnik-Chemical Process Engineering, Forckenbeckstraße 51, 52074 Aachen, Germany*

Abstract

Carbon based flow-electrodes are an increasing research field and find potential application in water treatment processes as well as energy conversion and storage. Flow-electrodes usually consist of a pumpable carbon slurry made of carbon particles suspended in a liquid electrolyte solution. One application for flow-electrodes is flow-electrode capacitive deionization (FCDI), which is a membrane-based, electrically-driven desalination method using mostly activated carbon as active material. In contrast to capacitive deionization (CDI) systems based on static electrodes, the use of flow-electrodes enables a continuous operation and the treatment of high salinity solutions. However, it was observed that the performance of FCDI processes heavily relies on the activated carbon quality. The process performance results from a wide range of parameters, including the activated carbon sample characteristics, which are usually not sufficiently covered and predicted by standard carbon analyses. With this article, we establish a foundation for applying electrochemical impedance spectroscopy (EIS) as predictive characterization method for flow-electrode materials. This includes the investigation of influencing system parameters and carbon characteristics, and the development of an equivalent circuit model. Finally, we demonstrate the possibility to predict and match the desalination performance of flow-electrodes based on different activated carbon types using EIS.

1. Introduction, Motivation and Objectives

The sustainable and reliant supply of sufficient water and energy to a growing population with increasing demand are major challenges humanity is facing, which calls for improved and new technologies. [1–4] A growing research field profiting from these challenges are flow-electrodes, which find potential application in the fields of

*Phone: +49-241-8095470, Fax: +49-241-8092252, Manuscripts.cvt@avt.rwth-aachen.de

water treatment and energy conversion and storage. [5] Flow-electrodes, also termed slurry electrodes [6], suspension electrodes [5] or fluidized bed electrodes [7], consist of conductive particles suspended in an electrolyte solution. The conductive particles can form percolating networks, which conduct electrons upon contact with the electrode or current collector and, thus, function as an electrode extension. Such flow-electrodes may be applied to support faradaic reactions, as required for electrosynthesis [8], batteries (e.g. zinc-air described in 1976 [9], lithium described in 2011 [10]), or for capacitive energy storage (flow capacitors, described in 2012 [11]) or capacitive salt adsorption for desalination (described in 2013 [12]).

Flow-electrode Capacitive Deionization. The latter, usually termed flow-electrode capacitive deionization (FCDI), is a promising application for flow-electrodes, which enables the removal of ionic species from solutions. [12, 13] It is based on the concept of capacitive deionization (CDI), which attracted increasing interest in the recent years due to its energy efficiency, the possibility of energy recovery and the potential application in selective ion removal and recovery of various ionic species. [4, 14–18] CDI uses an electrical field, which leads to the migration of ions towards the oppositely charged electrodes and finally the adsorption of ions in the electrical double layer (EDL) at the electrode surface. The desalination step can be compared to the charging of a capacitor, which enables an energy recovery during the regeneration. [19–21] However, due to the static electrodes applied in classical CDI systems, charge-discharge cycles are required, which limits the feasible salinity range to low salt concentrations. This limitation does not apply to FCDI, which enables a fully continuous operation due to the use of flowable electrodes recirculated through the module. [7, 22, 23] In case of a fully continuous operation, a diluate and concentrate stream of roughly constant concentrations are produced and the slurry electrode is

recirculated and regenerated continuously. Due to the combination of continuous operation and improved mass transport within the electrode, FCDI can treat even high-salinity water streams. [21] Additionally, the pumpability of the electrodes enables a range of new process layouts and applications. [24–26]

Flowable electrodes. All technologies based on such flowable (slurry-)electrodes rely heavily on the quality of the conductive material used to prepare the slurries. In most cases, these are carbon materials in various shapes and sizes. [5, 27] In case of applications with redox-active electrodes, materials with a comparably low surface area may be of advantage. Adsorption is not desired in this case, but rather a swift transport of the reacting components to the (flow-)electrode particle surface and a rapid transport of the products away from the surface. [28, 29] In case of technologies based on adsorption of components in the EDL, a high surface area is desirable. [14] Many different physical and chemical processes influence the performance of flow-electrodes in these processes, whose interactions are not fully understood yet. An increasing number of studies are investigating these interactions by means of modelling, [30, 31] imaging methods [32] and electrochemical characterization methods. [6, 11, 31, 33–36]

However, the influencing parameters and material characteristics on the performance as flow-electrode for specific applications still need further investigation. In most studies which focus on the investigation of slurry electrodes by electrochemical methods, such as cyclic voltammetry (CV) or electrochemical impedance spectroscopy (EIS), the flow-electrodes were investigated in a static manner. The slurries were filled into cells with various designs and analyzed. [5, 37–39] In some studies electrochemical methods were combined with rheological measurements performed in rheometers ("electro-rheology"), [5, 40, 41] and were, thus, investigated dynam-

ically. Only very few measurements were actually performed in a flow cell at dynamic conditions ("pumped flow-electrodes"). [31, 42] However, these measurements were mostly applied for qualitative comparisons and not analyzed and interpreted in depth. Hoyt et al. recently developed a first electrochemical impedance spectroscopy model, which matches experimental data of capacitive flow-electrodes. [31] In this study, Hoyt et al. developed a new circuit element, "Z_{EFC}", which simulates the suggested quasistatic behaviour of slurries at high frequencies.

Motivation and Objectives. The impact of specific material characteristics on the performance of a FCDI process is not fully understood yet. During the work with FCDI systems we observed significant differences in the performance of activated carbon (AC) provided by the manufacturers in different vessels in some cases, although supposedly of the same type. The actual rheology and desalination performance of a flowable electrode depends on a sum of parameters, such as particle size distribution, particle shape [43], particle conductivity [42], pore size distribution [44], carbon surface chemistry [45] and redox-activity [46]. These parameters can change drastically from batch to batch, depending on the carbon material. Most commercial carbons are not intended for the use as flowable electrodes and, thus, the standard specifications are usually not sufficient. Due to the focus on specific characteristics, most classical physical and chemical characterization methods have only limited significance for the evaluation of a carbon material for application in FCDI. Additionally, many of these methods, such as gas adsorption measurements, are very time-consuming. Hence, for an actual application, a reliable method for the evaluation of the overall performance of a carbon material as flowable electrode is required, which is able to produce results swiftly.

Electrochemical impedance spectroscopy (EIS) is an electrochemical characterization method, which applies an alternating potential (or current) of different frequencies to any electrochemical or material system, while the current (or voltage) response is recorded. The change of amplitude and the phase shift of the measured response allows to draw conclusions regarding chemical and physical processes dominating the system. The hypothesis behind this work is that EIS measurements can predict the desalination performance of slurries accurately when performed at dynamic conditions. EIS measurements allow conclusions regarding the most important material characteristics required for FCDI, when combined with classical physical and chemical characterization methods. While Hoyt et al. [31] took a first step and developed a model providing detailed physical understanding using a new circuit element, we use a more application oriented approach based on standard elements used in EIS models.

The aim of this study is to establish a foundation for an application of EIS as predictive characterization method for flow-electrode materials, e.g. for use as method for incoming goods inspection. This study includes the investigation of (1) the influence of different system parameters on the EIS response and (2) the development of a simple equivalent circuit model, which matches all obtained experimental results. We then go a step further by (3) examining the main influencing carbon characteristics on the FCDI performance, and (4) demonstrating the possibility to predict and match the desalination performance of flow-electrodes based on two completely different activated carbon types using EIS.

2. Materials and Methods

All experiments were performed with the same FCDI cell design as described in previous work. [21] The FCDI cells consist of polyethylene end plates, flat gas-

kets, epoxy-impregnated graphite electrodes (Müller & Rössner GmbH & Co. KG, 180x180x10 mm) with flow channels for the flow-electrodes (3 mm width, 2 mm depth, 200 cm overall length), a pair of cation and anion exchange membranes (Fumasep FKB-PK-130/ED-100 and Fumasep FAB-PK-130/ED-100, Fumatech BWT GmbH) with an effective surface area of 121 cm^2 and a 0.5 mm mesh spacer (Fumatech BWT GmbH, ED-100). A section of the cell is depicted in a cross-sectional view in Figure 1.

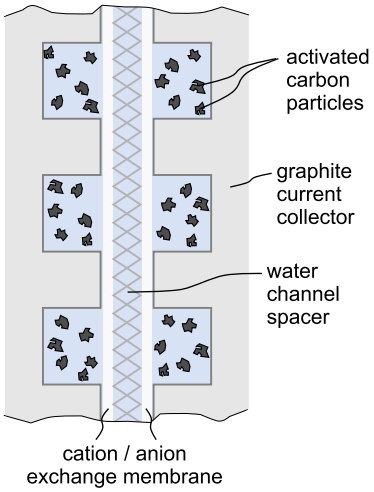

Figure 1. Section of the FCDI cell applied for EIS measurements and desalination measurements in cross-sectional view.

The feed water was supplied to the FCDI cells by a peristaltic pump (Ismatec Reglo ICC peristaltic pump with two independent channels). The salt solutions used as feed water and for the slurry preparation were prepared with purified water and 60 g/L sodium chloride (VWR Chemicals, >99.8%). The flow-electrodes were recirculated through the FCDI systems using a second peristaltic pump (Ismatec MCP process drive, Masterflex two-channel pump head Easy-Load II, Norprene tubing). All in all, four different activated carbon powder samples were applied in this work:

(1) Carbopal SC11PG, (2) Carbopal CCP1400 spezial (both provided by Donau Carbon GmbH, Germany) and (3)/(4) Norit D10 (Alfa Aesar), of which two different samples (hereafter termed "*Batch* 1" and "*Batch* 2") were analyzed, which were purchased in two different vessels, but had the same LOT number. Table 1 gives an overview of the activated carbon sample properties according to conventional characterization techniques, as provided by the manufacturers.

Table 1. Overview of activated carbons applied in this study. Information provided by the suppliers.

		Carbopal SC11PG	Carbopal CCP1400 spezial	NoritD10 -*Batch*1	NoritD10 -*Batch*2
abbreviations		SC	CCP	N-*B*1	N-*B*2
BET surface	**m^2/g**	950	1400	600	600
particle size	**d90**	64 μm	80 μm	140 μm	140 μm
	d50	16 μm	-	30 μm	30 μm
pH value	-	4.5 - 6.5	6 - 8	alkaline	alkaline
type	-	charcoal	coconut shell	-	-

2.1. Sieving experiments

The activated carbon was sieved at low amplitude in a sieving tower assembled of stackable sieves (Retsch GmbH, Germany) with mesh widths (in μm) of 20, 32, 40, 63, 80, 112, 125, 160, 230 and 350. The vibrating unit (Retsch AS200 digit) was set to 1.5 for the duration of each sieving interval. The mass of the particle fractions was measured at regular time intervals, sieving was stopped when no significant changes were observed in the mass of the particle fractions.

2.2. BET/gas sorption

The activated carbon samples (about 0.1 g each) were analyzed regarding their surface and porosity characteristics via N_2 gas adsorption/desorption measurements (ASAP 2020, Micromeritics). The samples were pretreated at 90 °C and 10 mbar for 24 h and degassed for 6 to 8 hours before the adsorption/desorption analysis.

2.3. Rheological Measurements

The rheological measurements were performed with a modular compact rheometer (MCR) from Anton Paar with the PP50 plate-plate measuring system at 25 °C. Shear rates between 10 1/s and 1000 1/s were applied.

2.4. Electrochemical impedance spectroscopy measurements

The electrochemical impedance spectroscopy (EIS) measurements were performend in two-electrode configuration with one FCDI cell through which two flow-electrodes were continuously recirculated from small glass beakers, which were continuously stirred. The experimental settings are summarized in Table 2. In case of the EIS measurements for the prediction of the desalination performance of a specific flow-electrode, the slurry was recirculated through both the desalination and concentration cells, as illustrated in Figure 2. The impedance measurements were performed with the desalination cell only. The EIS measurements were performed with a potentiostat with inbuilt frequency response analysis (FRA)-module (Reference 3000, Gamry). Frequencies between 0.009 and 10000 Hz were applied with an amplitude of 10 mV, experiments were performed without potential bias. In most measurements, the imaginary part was negative at high frequencies (above 1000), likely due to inductive effects of the cables. These effects were not considered in this work.

Table 2. Overview of parameter settings for EIS experiments.

	Slurry			**Feed water**	
	AC conc.	NaCl conc.	Flow rate	NaCl conc.	Flow rate
Figure no.	wt.%	g/L	mL/min	g/L	mL/min
Influence of activated carbon concentration and slurry flow rate					
3 (a)	0-10	60	150	60	13
3 (b)	10	60	0-150	60	13
Comparison of four activated carbons					
10 (a)	16	60	150	60	13
Prediction of desalination performance					
12 (a)	10, 15, 30, 35	60	175	60	2
12 (c)	17	60	175	60	2

2.5. Desalination experiments

A three-channel power supply (HM8143, HAMEG Instruments GmbH) was applied for the desalination measurements. The electrical conductivity (EC) of the aqueous solutions was measured using conductivity sensors (LTC0,35/23; Sensortechnik Meinsberg). Additionally, product water samples were taken during steady state operation. The density of each sample was analyzed to verify the salt concentration of the samples. The diluate stream and the concentrate stream were each treated in single-pass mode, while the flow-electrodes were recirculated at a constant flow-rate. The experimental settings for the desalination experiments (Figures 12 (b) and (d)) equal the settings given in Table 2 for Figures 12 (a) and (c).

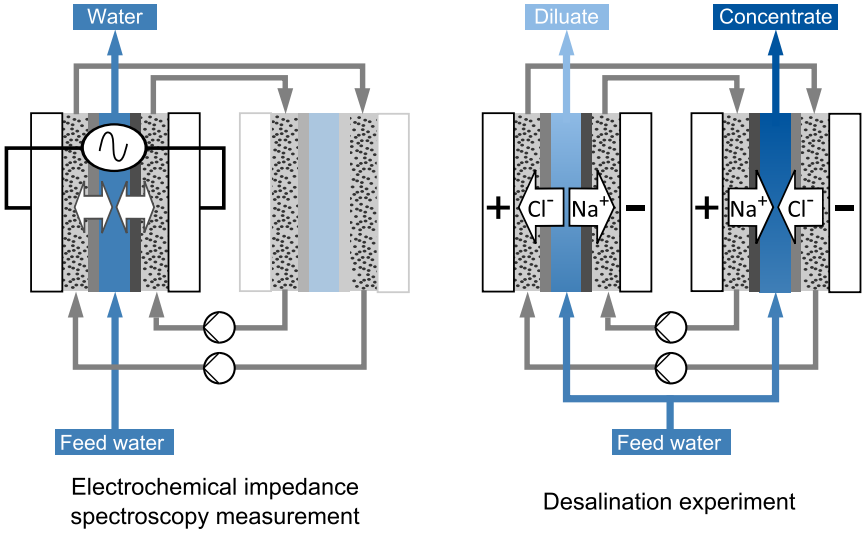

Figure 2. Illustration of the FCDI system layout applied for (left) the electrochemical impedance spectroscopy measurements and (right) the desalination experiments. The EIS measurements were performed with the desalination cell only. The desalination experiments were performed with the continuous two module FCDI layout described in previous publications. [21]

3. Results: EIS with Parameter Variations

As mentioned before, there are not many studies published in which the results of dynamic EIS measurements in an actual flow cell are described. For an initial understanding of the behaviour of such systems, parameter studies were performed, some results of which are plotted in Figure 3 (a) and (b). The experiments described in this section were performed with the activated carbon Carbopal SC11PG.

3.1. Influence of the activated carbon content

The activated carbon content was varied between 0-16 wt.%, while all other parameters were kept constant (Table 2). When considering the results plotted in Figure 3 (a), significant changes can be observed due to the addition of increasing amounts of activated carbon to the flow-electrode. At 0 wt.% activated carbon only

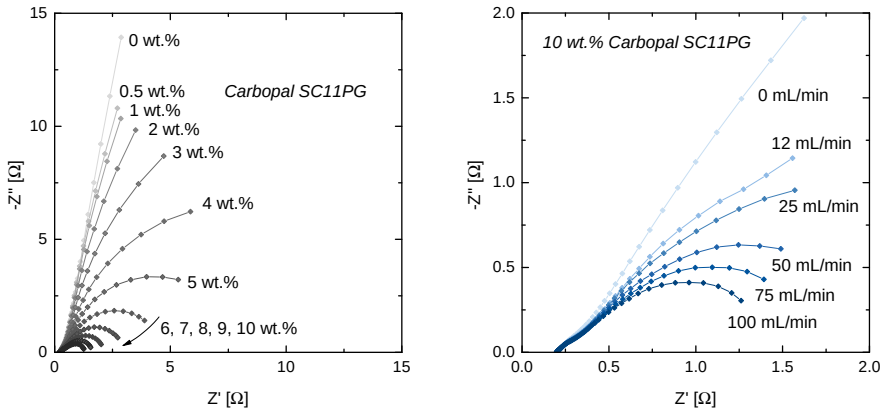

(a) Variation of the AC content. (b) Flow-electrode flow rate variation.

Figure 3. Results of EIS measurements; (a) Variation of the activated carbon (AC) content with a constant NaCl concentration of 60 g/L in both water channel and flow-electrode and a flow-electrode flow rate of 150 mL/min, and (b) Variation of the flow-electrode flow rate at a carbon loading of 16 wt.% (Carbopal SC11PG) and a 60 g/L NaCl concentration in both, water channel and flow-electrode.

a small shoulder is seen in the plot at high frequencies and a more or less straight line at an angle of around 80° towards the low frequencies, which is in agreement with the behaviour of rough electrode surfaces (non-ideal capacitance). A slightly depressed semicircle develops in the lower frequency range with the addition of activated carbon. With increasing activated carbon content, this semicircle becomes smaller, which correlates with an increasing capacitance and a decreasing interfacial resistance within the flow electrode.

3.2. Influence of the flow-electrode flow rate

Next, we investigated the transition in the impedance of static flow-electrodes to pumped flow-electrodes by varying the flow-electrode flow rate between 0-100 mL/min. All other parameters were kept constant (Table 2). The results are plotted in Fig-

ure 3 (b). At first sight, the changes to the Nyquist plot when increasing the flow-electrode flow rate look similar to the changes when increasing the activated carbon concentration. Without pumping, only a small shoulder is seen in the plot at high frequencies and a more or less straight line at an angle of around 55° towards the low frequencies, similar to the plot without activated carbon in the flow-electrode. In both cases, 0% activated carbon and 0 mL/min, the system acts like a static capacitor. The added activated carbon in the 0 mL/min case leads to a decrease of the line angle at low frequencies, which we explain by the influence of the activated carbon porosity. With increasing flow rate a slightly depressed semicircle forms at the lower frequency range, which correlates with an improved charge percolation. Our theories regarding these phenomena are discussed further in the following section.

4. Development of an equivalent electric circuit model

An equivalent circuit was developed, which can be used to fit and improve the understanding of the EIS data. The term equivalent circuit refers to a system of electric circuit elements, in this case, which imitates the impedance behaviour of an electrochemical system (an FCDI cell in this case) over a wide range of frequencies. According to Fletcher et al. [47], this represents the "electrochemist's way" of speaking.

In most EIS measurements with FCDI systems, mainly two semicircles were visible in the resulting Nyquist plots, which corresponds with two dominant time constants in the system (e.g. each one R-C element). In an FCDI system, we expect the EIS spectra to be influenced by both, diffusion limitation as well as the porous electrode material. In fact, the observed semicircles do not appear as perfect circles, but are rather depressed, which indicates an overlapping of the above mentioned

physical effects. In the following, the thoughts which led to the development of the equivalent circuit model presented in this article are illustrated in more detail.

4.1. Convectional current- formation of the low frequency semicircle

When transfering the understanding of faradaic systems and the understanding of the behaviour of classical capacitive systems (e.g. electrical double-layer supercapacitors) to capacitive flow-electrodes, the formation of the "larger", low frequency, semicircle can be explained. One might assume at a first thought that capacitive flow-electrodes in a FCDI cell, as applied in this study, would behave similar to a regular electrochemical double-layer capacitor (EDLC). This is the case for stagnant flow-electrodes or a FCDI cell with water or salt solution pumped through the flow-electrode channels. In these cases, as sketched in Figure 6, a semicircle is visible at the higher frequency range, which changes into a more or less linear dependence at the lower frequencies, with a slope of different angles, depending on the experimental conditions. However, in case the flow-electrode channel contains an activated carbon suspension and is pumped, a second semicircle appears in the low frequency region (Figure 4, Figure 3 (a) and (b)).

Such low-frequency semicircles are also visible in previously published work [42] and was also adressed by Hatzell et al. [5]. In the latter work, it was suggested that this behaviour observed for flow-electrodes results from increased electronical conductivity. Hoyt et al. [31] mentioned this as "current induced by convection". We agree that this behaviour is induced by electron transfer, which also leads to a "loss" of electrons in case of convective transport due to pumped flow-electrodes, as illustrated in Figure 4. The formation of similar semicircles in impedance spectra can be observed in case of faradaic reactions, which involve a transfer of electrons and are usually modelled by a R-C element, where the resistor is usually termed

charge transfer resistance.

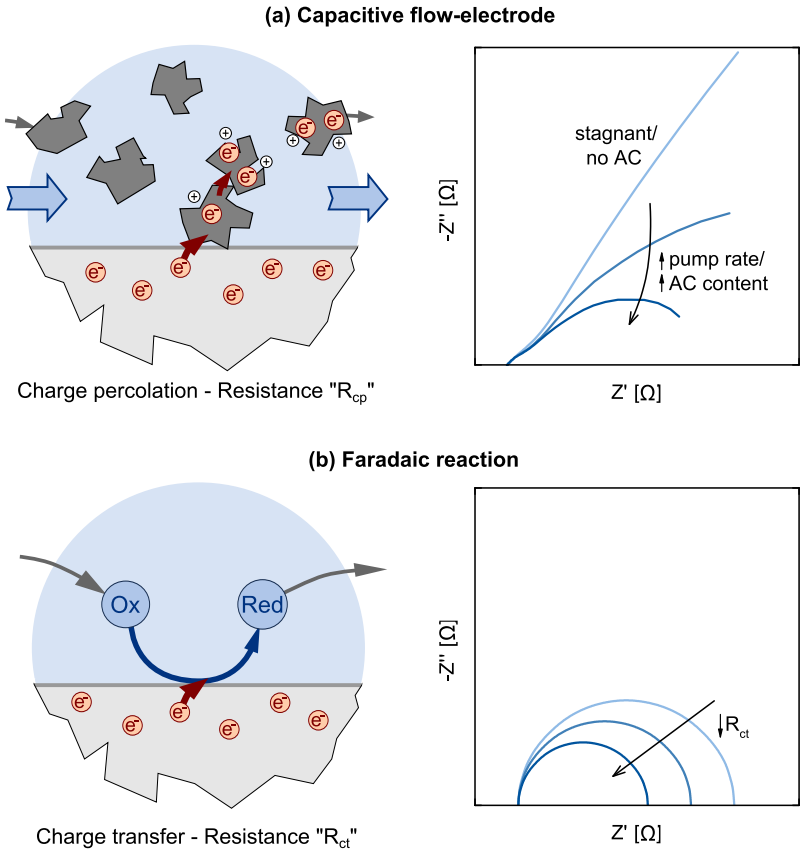

Figure 4. Illustration of (a) the effect of an electric current induced by convection on EIS spectra of a system based on capacitive flow-electrodes, and comparison to (b) an electrochemical system with faradaic reactions.

In case of capacitive flow-electrodes, when no potential bias is applied and when assuming ideal circumstances, no faradaic reactions should take place. The particles suspended in the salt solution are expected to be charged upon contact with the current collector or other charged particles (formation of charge percolation networks), which results in the adsorption of ions at the particle surface. This would usually result in the exhibition of a capacitive behaviour in the impedance spectra. In case

of an activated carbon concentration of 0 % (Figure 3 (a)) this is the case, as only the current collector is charged and no electrons are removed by pumping. This is also the case for stagnant carbon flow-electrodes. However, once the flow-electrodes are pumped, the particles are charged and some of them will leave the cell in a charged state, without the ability to be discharged again directly, as illustrated in Figure 4. Although the charge is stored capacitively, the measuring system, thus, records an apparent electric current caused by the convective charge removal. Due to the apparent electron flow, this phenomenon can be modelled using a resistor. The value of this resistor, which we will term as "charge percolation resistance R_{cp}" from here onwards, decreases with increasing conductivity of the flow-electrode. An increasing activated carbon content, for example, leads to an increased size of charge percolation networks [32] and an overall improved conductivity, which agrees with the discussion by Hatzell et al. [5].

4.2. Charge transfer at current collector- formation of the high frequency semicircle

Charge transfer phenomena at the current collector and insufficient contacting often lead to the observation of semicircles in the higher frequency range in Nyquist plots, for example in case of EDLCs [48, 49]. In case of FCDI, charge transfer at the current collector may include the graphite plate itself, as well as activated carbon particles resting at the surface, which are in direct contact with the graphite plate, as illustrated in Figure 5.

The results of fitting the equivalent circuit model to the experimental results shown in Figure 3, given in Tables S1 and S2, support this hypothesis. Due to the direct contact of the particles with the current collector, short ways and comparably small electrically active surface area lead to a comparably low resistance and capacitance. The magnitude of the capacitance and resistance influences the time constant

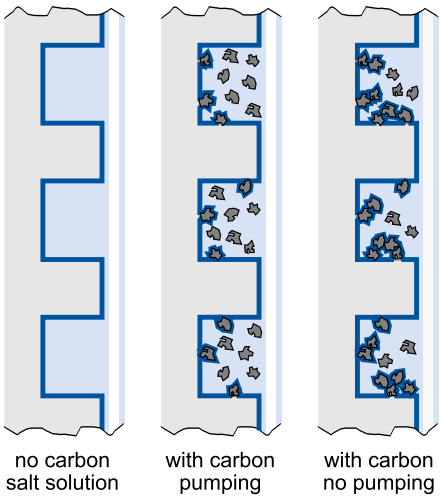

Figure 5. Illustration of carbon particles in direct contact with the current collector in case of three different experimental conditions. Charged surfaces due to direct contact with the current collector are highlighted in blue. This leads to a change in the capacitance C_{CC}, as can be seen in the values fitted to experimental results (Tables S1 and S2).

of a circuit element, which is in direct relation with the characteristic frequency of the related phenomenon. For simple R-C-circuits the time constant τ is defined as given in Equation 1, with R being the ohmic resistance and C being the capacitance of the correlating circuit elements. [50]

$$\tau = R \cdot C \tag{1}$$

In case of a small resistance and a small capacitance, the time constant is small, which leads to a high characteristic frequency.

4.3. Diffusion and electrode porosity- curve depression

We assume that the combined effect of diffusion and electrode porosity in the system lead to the non-ideal, depressed shape of the semicircles in the Nyquist plots

of experimental results regarding FCDI systems obtained in this work. Distinction between diffusion and porosity is not feasible with EIS, both cause a 45° line in impedance spectra in ideal cases. Due to the above discussed effect of the charge percolation resistance, this 45° line results in depressed semicircles in case of FCDI, as illustrated in Figure 6. While diffusion is usually modelled using Warburg elements, [51] electrode porosity is often modelled using different types of ladder networks, or so-called transmission lines. [47, 52] Robert de Levie [53, 54] provided the basis for modelling the behaviour of rough and porous electrodes by introducing the concept of the so-called "RC transmission lines" in the 1960s. [53, 54] Such transmission lines can be degenerated to models with ladder structures of different kinds, which can also model non-uniform porosity, as it occurs in materials based on natural raw materials, such as activated carbon. [47] Degenerate equivalent circuits are networks of electrical circuit elements with different structures, but the same total impedance behaviour over the investigated range of frequencies. [47] The disadvantage of such ladder structures is the high number of parameters, which need to be fitted. If the system is not well-known, the parameters need to be guessed, which hardly conveys an actual physical meaning. This, in combination with the fact that the observed flow-electrodes not only exhibit porous behaviour, but also diffusive behaviour, led us to choose a constant phase element as simplified (and artificial) circuit element representing the systems porosity as well as diffusion behaviour. A constant phase element can, in fact, be seen as an infinite ladder network ranging over an infinite range of time constants. However, in our measurements we often observed that an "unrestrained" constant phase element does not model the system very well, which leads to the conclusion that the system is not limited by porosity or diffusion at low frequency. To constrain this behaviour to a smaller frequency range we, thus, used a charge percolation resistance in parallel to the constant phase element, which leads

305 to the behaviour illustrated in Figure 6.

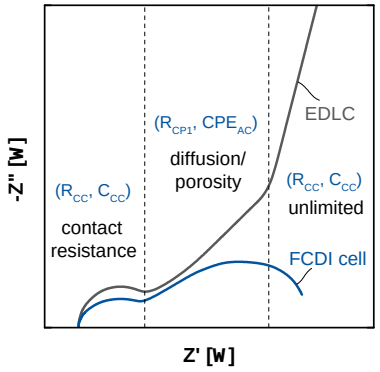

Figure 6. Typical Nyquist plots of supercapacitors and capacitive flow electrodes and indicated physical behavioural regimes.

306 *4.4. The equivalent circuit model: Putting it together*

307 By combining the above discussed observations, we developed the equivalent cir-
308 cuit illustrated in Figure 7. We found that this equivalent circuit can be fitted to
309 represent measurements with FCDI systems in a wide range of settings regarding
310 different parameters such as activated carbon content and flow-electrode flow rate
311 with a minimum of fitting parameters.

312 The circuit elements depicted in Figure 7 represent (1) the electron transfer at
313 the current collector (R_{CC} and C_{CC}), (2) the influence of diffusion and electrode
314 porosity (R_{cp1} and CPE_{AC}), (3) the capacitance and current induced by convection
315 (R_{cp2} and C_{dl}) and (4) the combined, serial resistance of solutions, membranes etc.
316 (R_S).

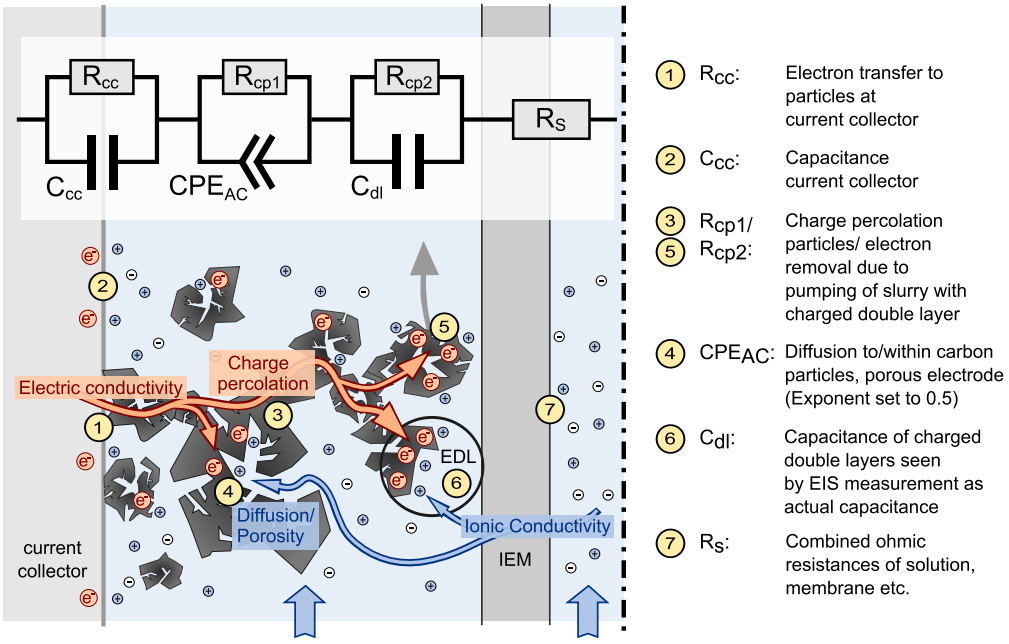

Figure 7. Equivalent circuit model applied to fit experimental data.

5. Further results and discussion

5.1. Fit results and observations based on the equivalent circuit model

The equivalent circuit model shown in Figure 7 was fitted to experimental results by using the software ZView 2 (Version 3.5b, Scribner Associates, Inc.). The square of the standard deviation of the resulting fits from experimental results was in the range of 10^{-4} in most cases. Tables S1 and S2 of the supplementary materials show results for the fit values of the different elements of the equivalent circuit model, fitted to the results shown in Figure 3 (a) and (b).

Variation of the activated carbon content and flow-electrode flow rate. The circuit elements with the most significant changes due to a change in the activated carbon content are C_{CC}, R_{cp1}, R_{cp2} and C_{dl}. The changes in C_{CC} were discussed in Section 4.2

and illustrated in Figure 5. The values of R_{cp1} are mostly similar to R_{cp2}, which means the electrode porosity/diffusion has an influence over the whole frequency spectrum. In case of low activated carbon concentrations as well as low flow-electrode flow rate, the fitted values of R_{cp1} increase disproportionally. In this case, the constant phase element dominates also at lower frequencies. To model this behaviour, R_{cp1} was excluded from the model in case of low activated carbon contents and low flow-electrode flow rates. With an increasing activated carbon content the size of the charge percolation networks increases [32], which leads to an improved exploitation of the activated carbons maximum salt adsorption capacity as well as an improved conductivity. This leads to an increase of the double layer capacitance C_{dl} and a significant decrease of the charge percolation resistance R_{cp2}, which matches the fit results well. In case of an increasing flow-electrode flow rate, however, there is a sudden increase in C_{dl} from 0 mL/min to 12 mL/min, while at further increasing flow rate C_{dl} decreases again. In case of the stagnant flow-electrode (0 mL/min), not all particles get in contact with the current collector. Some of the particles "rest" in the bulk of the flow-electrode, not in contact with the current collector. When the flow-electrodes are pumped, the particles are moved and, thus, brought into contact with the current collector. A larger fraction of the maximum salt adsorption capacity is used. At even higher flow rates the capacitance apparently decreases, due to the removal of charged particles by pumping. In this case, the increased capacitance has an influence on the current induced by convection and, thus, a decrease of R_{cp2}. On the other hand, an increased flow-electrode flow rate, and thus a reduced residence time, may also lead to an incomplete charging of the pores, which may also reduce the value of C_{dl}. The overlap of these two effects may explain the maximum of R_{cp2} at a flow rate of 50 mL/min.

Variation of the salt concentration. Additional experiments were performed to investigate the influence of the electrode porosity/diffusion in capacitive flow-electrode systems. For this, EIS measurements were performed with varied NaCl concentrations at constant activated carbon concentration.

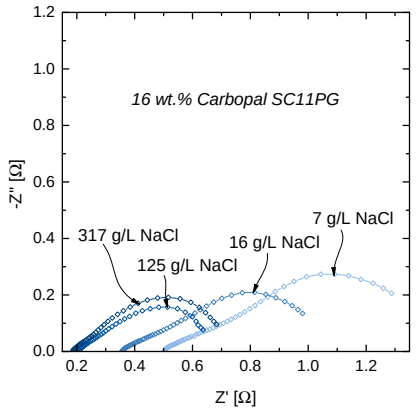

Figure 8. Results of EIS measurements; Variation of the NaCl concentration at a constant activated carbon content of 16 wt.% (Carbopal SC11PG) and a flow-electrode flow rate of 150 mL/min.

At a low NaCl concentration a strong semicircle depression at low frequencies as well as a quasi-linear region at the higher frequencies is visible, described as "quasi-steady porous electrode behaviour" by Hoyt et al. [31]. We agree that this behaviour is caused by electrode porosity/diffusion, which we chose to model with a constant phase element and a parallel resistor ("charge percolation resistance"). This way of modelling enables an influence of the porosity/diffusion limitation of the whole spectrum of frequencies, which leads to a better fit in the lower frequency range at relatively low flow-electrode flow rates compared to the nice newly-developed model by Hoyt et al. [31]. With increasing salt concentration, the low frequency semicircles become rounder and shift to higher frequencies. This effect may be explained by a reduced diffusion way at high salt concentrations and, thus, a faster charging, which

shifts the characteristic frequency of the low-frequency semicircle to higher frequencies. This correlates well with the fit results given in Table S4 of the supplementary material, which show a decreasing trend of the fit values of R_{cp2} and additionally a reduction of C_{dl}. The latter may be explained by an increase in the charge loss due to the convection-induced current at increasing salt concentrations.

5.2. The influence of the particle size

In the following, we investigate the origin of the observed performance differences between the four activated carbon samples. A set of experiments was performed comparing the results of impedance measurements to results from desalination experiments, which were all performed with the same set of parameters. Figure 9 (a) shows results of impedance measurements performed with the activated carbon Carbopal SC11PG and sieved particle size fractions of the same activated carbon. Figure 9 (b) shows results of the corresponding desalination experiments. While significantly different particle size fractions were chosen for the comparison, the difference in impedance as well as desalination performance is minute. The experiments performed with the size fraction of 40-50 μm show the most significant differences to the other measurements. The real as well as imaginary impedance are slightly increased, which matches the result of the desalination experiments, in which this fraction showed the lowest desalination rate. The microscopic images depicted in Figure S2 show significant differences between the different particle size fractions. However, in particle size fraction of 40-50 μm, for example, is still a significant number of small particles present, which may diminish the effect of sieving to a certain extent. All in all, the differences between the samples are unexpectedly low, and cannot explain the significant differences observed in the performance of different carbon batches.

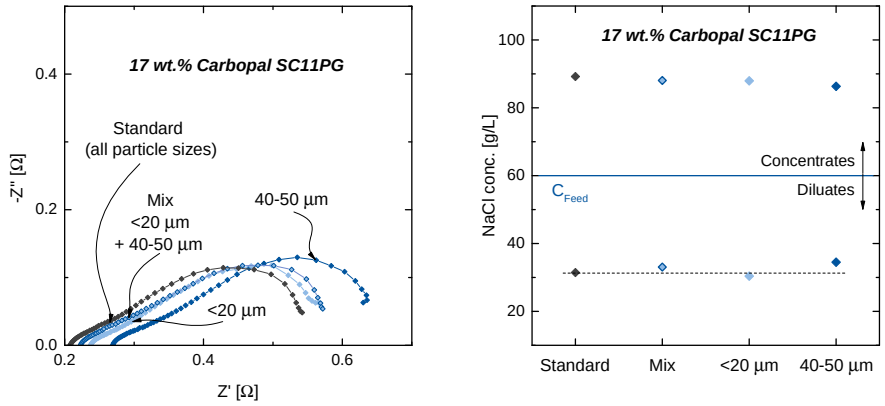

(a) Particle sizes - Nyquist plot. (b) Particle sizes- desalination.

Figure 9. Results of EIS measurements and desalination experiments; A sample of the activated carbon Carbopal SC11PG was sieved into different particle size fractions. The standard sample was compared to the size fractions <20 μm and 40-50 μm of the same activated carbon and a mixture of the two sieved fractions. The EIS response at the same weight percentage was measured and compared to the desalination performance.

5.3. Comparison of four AC samples: the origin of the performance differences

To identify the activated carbon characteristics with the main influence on the desalination performance, we compared four different activated carbons, as listed in the "Materials and Methods" section. The four samples exhibited significantly different results regarding desalination performance and impedance behaviour, as plotted in Figure 10 (a).

At the same mass percentage, the activated carbon slurry prepared with "Carbopal SC11PG" showed a lower impedance and resistance by more than a factor of six, compared to the carbon sample with the highest impedance. The fit results for C_{DL} and R_{CP2}, plotted in Figure 10 (b), show an inversed correlation between increasing capacitance and decreasing ohmic resistance. With decreasing resistance the capacitance increases, which may partially be due to an improved use of the avail-

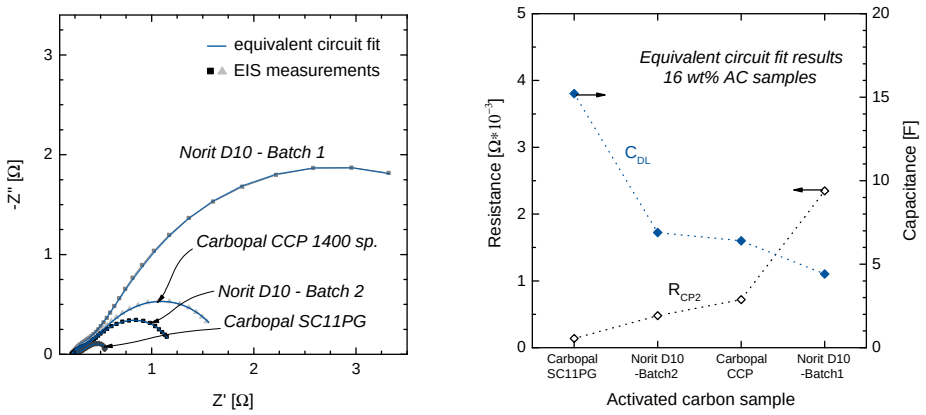

(a) EIS results. (b) EIS fit values.

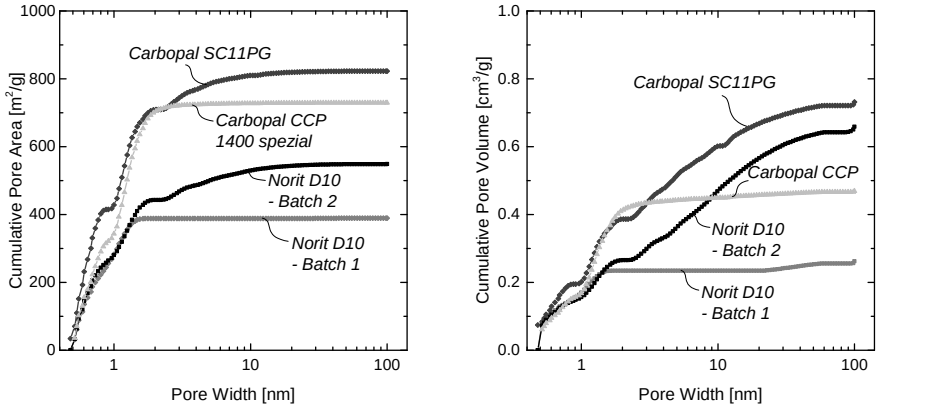

(c) Cumulative Pore Area. (d) Cumulative Pore Volume.

Figure 10. Comparison of four different activated carbon samples, results of (a) EIS measurements with 16 wt.% activated carbon sample, (b) fitted values using the equivalent circuit model, and (c)/(d) results of gas adsorption measurements to determine the pore size distribution.

able electrically active surface area. The results from gas adsorption measurements, plotted in Figures 10 (c) and (d), revealed the pore size distribution as cause of the differences. The pore size distribution also appears to be the main difference between the two different batches of the same activated carbon type. The two best performing carbons have a significant amount of mesopores. Especially the cumulative pore

volume, plotted in Figure 10 (d), correlates well with the desalination/impedance performance of the carbons, while the cumulative pore area does not. Two effects (Figure 11) can explain the improved desalination performance with the presence of mesopores: (1) an improved ion accessibility and transport and reduced transport resistance within mesopores and (2) a significantly increased outer particle volume, which leads to a significantly increased carbon volume fraction in the suspension at the same mass fraction. The increased "outer particle" volume fraction leads to a significant improvement in the charge percolation between particles, and a thus improved desalination performance. The increased viscosities observed in carbon slurries prepared with mesoporous carbons supports this hypothesis, as an increased volume fraction will also increase inner friction in the suspension. However, both effects may play an important role in the performance boost due to the presence of a significant amount of mesopores.

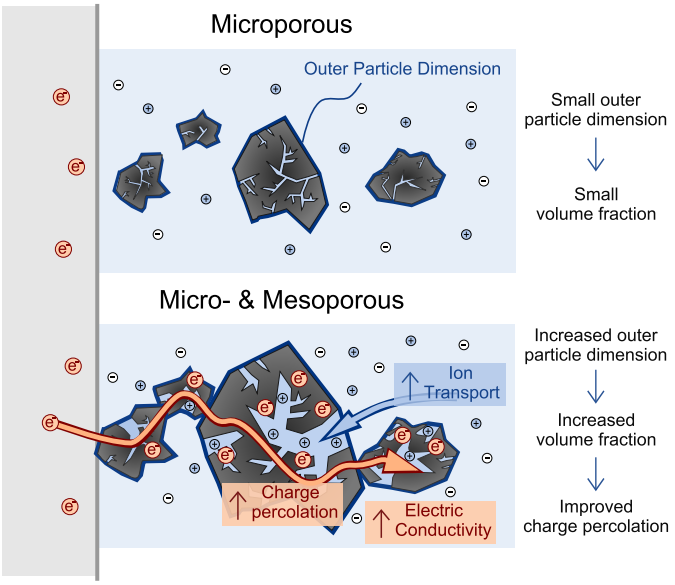

Figure 11. Charge and ion transport in carbon suspensions of microporous carbons and carbons with additional mesopores at equal carbon mass percentages.

In further works, the influence of internal and external diffusion should be investigated in more depth. A more detailed equivalent circuit model could help to differentiate between the mass transport limitations caused by the diffusion within the particle (internal diffusion) and the diffusion to the particle (outer diffusion). This would provide further scientific insight into the transport mechanisms in porous slurry electrodes and could help to further simplify the search for an optimized carbon material.

5.4. Prediction of the desalination performance with EIS

A final set of experiments aimed at demonstrating the possibility to predict the desalination performance of a carbon slurry by using EIS. We prepared flow-electrode suspensions using two activated carbons with significantly different characteristics, one being mainly microporous (Norit D10, Batch1, "Carbon A"), while the other also contains a significant amount of mesopores (Carbopal SC11PG, "Carbon B"). We adjusted the carbon content of the flow-electrodes to achieve a similar impedance behaviour with the two different carbon types at two concentration ranges. The results of this set of experiments are shown in Figure 12 (a). Finally, we demonstrated the relevance of the impedance results for the desalination performance by performing continuous desalination experiments with the two-module setup illustrated in Figure 2 (right side). Results of the desalination experiments are plotted in Figure 12 (b).

We achieved a good match in the impedance behaviour of Carbon A and Carbon B for the mass fractions of the sets 10 wt% A / 30 wt% B and 15 wt% A / 35 wt% B (Figure 12 (a)). The carbon slurries also showed matching results in the corresponding desalination experiments (Figure 12 (b)). In case of the higher percentage set of carbon slurries, 15 wt% A / 35 wt% B, a slightly more pronounced deviation

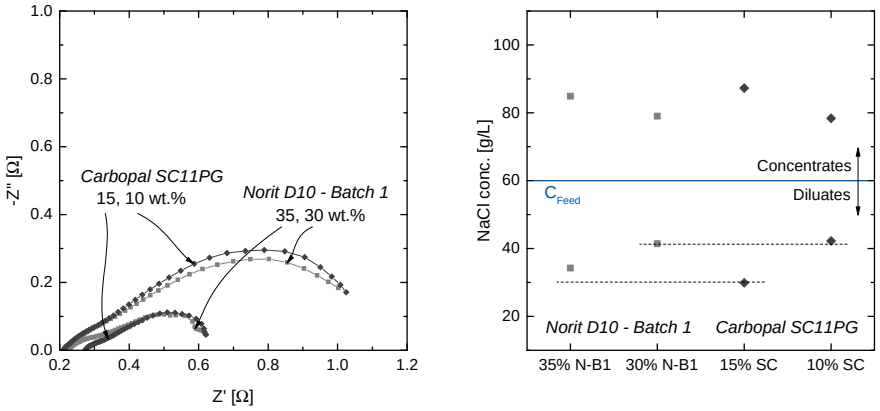

(a) Performance match - Nyquist plot. (b) Performance match - desalination.

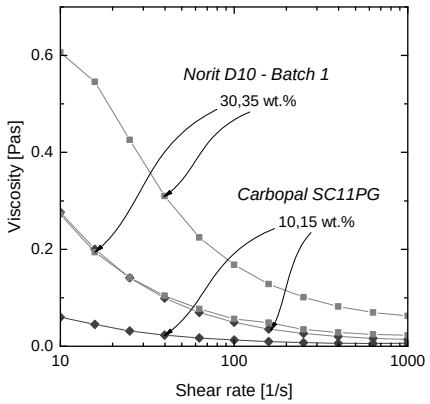

(c) Viscosity measurements.

Figure 12. Results of EIS measurements, desalination and viscosity experiments; Suspensions based on two different activated carbons were matched regarding their EIS response at two different mass fraction values and the corresponding desalination performance tested.

was observed between the desalination performances of the matched flow-electrodes. The 15 wt% slurry of Carbon B reached a somewhat better desalination compared to the 35 wt% slurry prepared with Carbon A. The curve representing the 15 wt% slurry of Carbon B intersects the x-axis at a higher ohmic resistance than the curve representing the 35 wt% slurry prepared with Carbon A, while the resistances at low

frequencies are nearly the same. This results in a small difference in the overall real impedance of around 0.034 Ω, which may explain the small difference in desalination performance between the two carbon slurries. However, all in all the results for the matched slurries matched well.

Figure 12 (c) shows results of a viscosity investigation performed with the above described carbon slurries, which were adapted in weight percentage in a way to exhibit a similar electrochemical performance. While the desalination performance of the two pairs of slurries match very well, the rheological behaviour appears to be significantly different. The slurries made of the Carbopal SC11PG carbon have a significantly lower viscosity, while reaching the same desalination performance. Hence, a combination of electrochemical impedance spectroscopy with rheological measurements is well suited for a screening study for activated carbons with optimum performance in FCDI processes.

6. Conclusions

In this article, we establish the foundation for EIS as a predicitve characterization method for flow-electrode materials, especially in the context of water treatment. We investigated the influence of different system parameters on the EIS response and developed an equivalent circuit model, which can be fitted to match all results we obtained experimentally. We investigated the influence of different carbon characteristics on the desalination performance and observed a significant influence of the pore size distribution. The carbon samples with a significant amount of mesopores, additional to micropores, showed an overall improved performance. The activated carbons with the highest cumulative pore volume showed the best desalination performance, which we conclude is mainly due to an increased volume fraction of the activated carbon. An increased carbon outer volume fraction leads to an improved

charge percolation and thus an improved desalination. On the other hand, the particle size distribution did not have a significant influence on the desalination performance. Finally, we demonstrated the possibility to use electrochemical impedance spectroscopy measurements to adjust the performance of flow-electrode suspensions made of different activated carbons. The desalination performance of the matched flow-electrodes showed a very good congruence. The results of this study are valuable for application as carbon characterization method for application in technologies using flow-electrodes. EIS may be applied for on-line process monitoring and control of the flow-electrode performance in various processes. It can also serve as direct, easy in-line method for the characterization of carbon suspensions in general, considering the actual wetting and agglomeration conditions in-situ.

Acknowledgements

This work was supported by the German Federal Ministry of Education and Research (BMBF) under the project ElektroWirbel (FKZ 13XP5008) and by the European Research Council (ERC) under the European Unions Horizon 2020 research and innovation program (694946). M.W. appreciates the funding from the Alexander von Humboldt Foundation. The authors thank Fumatech BWT GmbH and Donau Carbon GmbH for the provision of material samples. The authors thank Andreas Augustin and Benedikt Aumeier for the support in the development of the gas adsorption measurement method, and Jingyu Xie, Niklas Köller and Rachel Krupp for their constructive effort in this study. The authors thank Tomas Klicpera, Dana Kaubitzsch, Faras Brumand-Poor, Uwe Schnakenberg and Oliver Blatt for the valuable discussions.

References

[1] M. M. Mekonnen, A. Y. Hoekstra, Four billion people facing severe water scarcity, Science Advances (February) (2016) 1–7.

[2] M. Elimelech, W. a. Phillip, The future of seawater desalination: energy, technology, and the environment., Science (New York, N.Y.) 333 (6043) (2011) 712–717. doi:10.1126/science.1200488.

[3] B. Dunn, B. Dunn, H. Kamath, J.-m. Tarascon, Electrical energy storage for the gridfor the Grid : A Battery of choices, Science Magazine 334 (6058) (2011) 928–936. doi:10.1126/science.1212741.

[4] S. Y. Pan, S. W. Snyder, Y. J. Lin, P. C. Chiang, Electrokinetic desalination of brackish water and associated challenges in the water and energy nexus, Environmental Science: Water Research and Technology 4 (5) (2018) 613–638. doi:10.1039/c7ew00550d.

[5] K. B. Hatzell, M. Boota, Y. Gogotsi, Materials for suspension (semi-solid) electrodes for energy and water technologies, Chem. Soc. Rev. 44 (23) (2015) 8664–8687. doi:10.1039/C5CS00279F.
URL http://xlink.rsc.org/?DOI=C5CS00279F

[6] T. J. Petek, N. C. Hoyt, R. F. Savinell, J. S. Wainright, Characterizing Slurry Electrodes Using Electrochemical Impedance Spectroscopy, Journal of the Electrochemical Society 163 (1) (2015) A5001–A5009. doi:10.1149/2.0011601jes.
URL http://jes.ecsdl.org/cgi/doi/10.1149/2.0011601jes

[7] G. Doornbusch, J. Dykstra, P. Biesheuvel, M. Suss, Fluidized bed electrodes with high carbon loading applied to water desalination by capacitive deioniza-

tion, Submitted 00 (2015) 1–6. doi:10.1039/C5TA10316A.
URL http://dx.doi.org/10.1039/C5TA10316A

[8] J. R. Backhurst, J. M. Coulson, F. Goodridge, R. E. Plimley, M. Fleischmann, A Preliminary Investigation of Fluidized Bed Electrodes, Journal of The Electrochemical Society 116 (11) (1969) 1600. doi:10.1149/1.2411628.
URL http://jes.ecsdl.org/cgi/doi/10.1149/1.2411628

[9] A. J. Appleby, M. Jacquier, The C.G.E. circulating zinc/air battery: A practical vehicle power source, Journal of Power Sources 1 (1) (1976) 17–34. doi:10.1016/0378-7753(76)80003-1.

[10] M. Duduta, B. Ho, V. C. Wood, P. Limthongkul, V. E. Brunini, W. C. Carter, Y. M. Chiang, Semi-solid lithium rechargeable flow battery, Advanced Energy Materials 1 (4) (2011) 511–516. doi:10.1002/aenm.201100152.

[11] V. Presser, C. R. Dennison, J. Campos, K. W. Knehr, E. C. Kumbur, Y. Gogotsi, The electrochemical flow capacitor: A new concept for rapid energy storage and recovery, Advanced Energy Materials 2 (7) (2012) 895–902. doi:10.1002/aenm.201100768.

[12] S. I. Jeon, H. R. Park, J. G. Yeo, S. Yang, C. H. Cho, M. H. Han, D. K. Kim, Desalination via a new membrane capacitive deionization process utilizing flow-electrodes, Energy & Environmental Science 6 (5) (2013) 1471–1475. doi:Doi 10.1039/C3ee24443a.

[13] P. Ratajczak, M. E. Suss, F. Kaasik, F. Béguin, Carbon electrodes for capacitive technologies, Energy Storage Materials 16 (May 2018) (2019) 126–145.

doi:10.1016/j.ensm.2018.04.031.
URL https://doi.org/10.1016/j.ensm.2018.04.031

[14] Y. Oren, Capacitive deionization (CDI) for desalination and water treatment - past, present and future (a review), Desalination 228 (1-3) (2008) 10–29. doi:10.1016/j.desal.2007.08.005.

[15] M. a. Anderson, A. L. Cudero, J. Palma, Capacitive deionization as an electrochemical means of saving energy and delivering clean water. Comparison to present desalination practices: Will it compete?, Electrochimica Acta 55 (12) (2010) 3845–3856. doi:10.1016/j.electacta.2010.02.012.
URL http://dx.doi.org/10.1016/j.electacta.2010.02.012

[16] S. Porada, R. Zhao, A. Van Der Wal, V. Presser, P. M. Biesheuvel, Review on the science and technology of water desalination by capacitive deionization, Progress in Materials Science 58 (8) (2013) 1388–1442. doi:10.1016/j.pmatsci.2013.03.005.
URL http://dx.doi.org/10.1016/j.pmatsci.2013.03.005

[17] M. E. Suss, Size-Based Ion Selectivity of Micropore Electric Double Layers in Capacitive Deionization Electrodes, Journal of The Electrochemical Society 164 (9) (2017) E270–E275. arXiv:1704.04156, doi:10.1149/2.1201709jes.
URL http://jes.ecsdl.org/lookup/doi/10.1149/2.1201709jes

[18] E. Hack, D. Hümmer, M. Franzreb, Concentration of crotonic acid using capacitive deionization technology, Separation and Purification Technology 209 (September 2018) (2019) 658–665. doi:10.1016/j.seppur.2018.08.049.
URL https://doi.org/10.1016/j.seppur.2018.08.049

[19] P. Długołecki, A. Van Der Wal, Energy recovery in membrane capacitive

deionization, Environmental Science and Technology 47 (9) (2013) 4904–4910. doi:10.1021/es3053202.

[20] S.-i. Jeon, J.-g. Yeo, S. Yang, J. Choi, D. K. Kim, Ion storage and energy recovery of a flow-electrode capacitive deionization process, Journal of Materials Chemistry A 2 (18) (2014) 6378. doi:10.1039/c4ta00377b.

[21] A. Rommerskirchen, C. J. Linnartz, D. Müller, L. K. Willenberg, M. Wessling, Energy Recovery and Process Design in Continuous FlowElectrode Capacitive Deionization Processes, ACS Sustainable Chemistry & Engineering (2018) acssuschemeng.8b02466doi:10.1021/acssuschemeng.8b02466.
URL http://pubs.acs.org/doi/10.1021/acssuschemeng.8b02466

[22] Y. Gendel, A. K. E. Rommerskirchen, O. David, M. Wessling, Batch mode and continuous desalination of water using flowing carbon deionization (FCDI) technology, Electrochemistry Communications 46 (2014) 152–156. doi:10.1016/j.elecom.2014.06.004.

[23] A. Rommerskirchen, Y. Gendel, M. Wessling, Single module flow-electrode capacitive deionization for continuous water desalination, Electrochemistry Communications 60 (2015) 34–37. doi:10.1016/j.elecom.2015.07.018.

[24] C. Linnartz, A. Rommerskirchen, M. Wessling, Y. Gendel, Flow-electrode capacitive deionization for double displacement reactions, ACS Sustainable Chemistry & Engineering (5) (2017) 3906–3912. doi:10.1021/acssuschemeng.6b03086.

[25] P. Nativ, O. Lahav, Y. Gendel, Separation of divalent and monovalent ions using flow-electrode capacitive deionization with nanofiltration membranes, Desalina-

tion 425 (October 2017) (2018) 123–129. doi:10.1016/j.desal.2017.10.026.
URL http://dx.doi.org/10.1016/j.desal.2017.10.026

[26] C. Zhang, J. Ma, D. He, T. D. Waite, Capacitive Membrane Stripping for Ammonia Recovery (CapAmm) from Dilute Wastewaters, Environmental Science and Technology Letters 5 (1) (2018) 43–49. doi:10.1021/acs.estlett.7b00534.

[27] S. Yang, H.-r. Park, J. Yoo, H. Kim, J. Choi, M. H. Han, D. K. Kim, Plate-Shaped Graphite for Improved Performance of Flow-Electrode Capacitive Deionization, Journal of The Electrochemical Society 164 (13) (2017) E480–E488. doi:10.1149/2.1551713jes.
URL http://jes.ecsdl.org/lookup/doi/10.1149/2.1551713jes

[28] K. Percin, A. Rommerskirchen, R. Sengpiel, Y. Gendel, M. Wessling, 3D-printed conductive static mixers enable all-vanadium redox flow battery using slurry electrodes, Journal of Power Sources 379 (January) (2018) 228–233. doi:10.1016/j.jpowsour.2018.01.061.
URL https://doi.org/10.1016/j.jpowsour.2018.01.061

[29] H. Parant, G. Muller, T. Le Mercier, J. M. Tarascon, P. Poulin, A. Colin, Flowing suspensions of carbon black with high electronic conductivity for flow applications: Comparison between carbons black and exhibition of specific aggregation of carbon particles, Carbon 119 (2017) 10–20. doi:10.1016/j.carbon.2017.04.014.

[30] N. C. Hoyt, R. F. Savinell, J. S. Wainright, Modeling of flowable slurry electrodes with combined faradaic and nonfaradaic currents, Chemical Engineering Science 144 (2016) 288–297. doi:10.1016/j.ces.2016.01.048.
URL http://dx.doi.org/10.1016/j.ces.2016.01.048

[31] N. C. Hoyt, E. Agar, E. A. Nagelli, R. Savinell, J. Wainright, Editors' Choice-Electrochemical Impedance Spectroscopy of Flowing Electrosorptive Slurry Electrodes, Journal of The Electrochemical Society 165 (10) (2018) E439–E444. doi:10.1149/2.0051810jes.
URL http://jes.ecsdl.org/lookup/doi/10.1149/2.0051810jes

[32] K. B. Hatzell, J. Eller, S. L. Morelly, M. H. Tang, N. J. Alvarez, Y. Gogotsi, Direct observation of active material interactions in flowable electrodes using X-ray tomography, Faraday Discuss. 199 (2017) 511–524. doi:10.1039/C6FD00243A.
URL http://xlink.rsc.org/?DOI=C6FD00243A

[33] K. B. Hatzell, M. Beidaghi, J. W. Campos, C. R. Dennison, E. C. Kumbur, Y. Gogotsi, A high performance pseudocapacitive suspension electrode for the electrochemical flow capacitor, Electrochimica Acta 111 (2013) 888–897. doi:10.1016/j.electacta.2013.08.095.
URL http://dx.doi.org/10.1016/j.electacta.2013.08.095

[34] C. R. Dennison, M. Beidaghi, K. B. Hatzell, J. W. Campos, Y. Gogotsi, E. C. Kumbur, Effects of flow cell design on charge percolation and storage in the carbon slurry electrodes of electrochemical flow capacitors, Journal of Power Sources 247 (2014) 489–496. doi:10.1016/j.jpowsour.2013.08.101.

[35] C. R. Dennison, Y. Gogotsi, E. C. Kumbur, In situ distributed diagnostics of flowable electrode systems: Resolving spatial and temporal limitations, Physical Chemistry Chemical Physics 16 (34) (2014) 18241–18252. doi:10.1039/c4cp02820a.

[36] T. J. Petek, N. C. Hoyt, R. F. Savinell, J. S. Wainright, Slurry electrodes for

iron plating in an all-iron flow battery, Journal of Power Sources 294 (2015) 620–626. doi:10.1016/j.jpowsour.2015.06.050.

[37] F. Y. Fan, W. H. Woodford, Z. Li, N. Baram, K. C. Smith, A. Helal, G. H. McKinley, W. C. Carter, Y. M. Chiang, Polysulfide flow batteries enabled by percolating nanoscale conductor networks, Nano Letters 14 (4) (2014) 2210–2218. doi:10.1021/nl500740t.

[38] K. Y. Choo, C. Y. Yoo, M. H. Han, D. K. Kim, Electrochemical analysis of slurry electrodes for flow-electrode capacitive deionization, Journal of Electroanalytical Chemistry 806 (2017) 50–60. doi:10.1016/j.jelechem.2017.10.040.
URL http://dx.doi.org/10.1016/j.jelechem.2017.10.040

[39] B. Akuzum, L. Agartan, J. Locco, E. C. Kumbur, Effects of particle dispersion and slurry preparation protocol on electrochemical performance of capacitive flowable electrodes, Journal of Applied Electrochemistry 47 (3) (2017) 369–380. doi:10.1007/s10800-017-1046-5.

[40] H. Block, J. P. Kelly, Electro-rheology, Journal of Physics D: Applied Physics 21 (1988) 1661–1677.

[41] M. Youssry, L. Madec, P. Soudan, M. Cerbelaud, D. Guyomard, B. Lestriez, Formulation of flowable anolyte for redox flow batteries: Rheo-electrical study, Journal of Power Sources 274 (2015) 424–431. doi:10.1016/j.jpowsour.2014.10.076.

[42] P. Liang, X. Sun, Y. Bian, H. Zhang, X. Yang, Y. Jiang, P. Liu, X. Huang, Optimized desalination performance of high voltage flow-electrode capacitive deionization by adding carbon black in flow-electrode, Desalination 420 (May)

(2017) 63–69. doi:10.1016/j.desal.2017.05.023.
URL http://linkinghub.elsevier.com/retrieve/pii/S0011916416320847

[43] M. Boota, K. B. Hatzell, M. Beidaghi, C. R. Dennison, E. C. Kumbur, Y. Gogotsi, Activated Carbon Spheres as a Flowable Electrode in Electrochemical Flow Capacitors, Journal of the Electrochemical Society 161 (6) (2014) A1078–A1083. doi:10.1149/2.072406jes.
URL http://jes.ecsdl.org/cgi/doi/10.1149/2.072406jes

[44] M. Tian, Y. Sun, C. J. Zhang, J. Wang, W. Qiao, L. Ling, D. Long, Enabling high-rate electrochemical flow capacitors based on mesoporous carbon microspheres suspension electrodes, Journal of Power Sources 364 (2017) 182–190. doi:10.1016/j.jpowsour.2017.08.001.
URL http://dx.doi.org/10.1016/j.jpowsour.2017.08.001

[45] K. B. Hatzell, M. C. Hatzell, K. M. Cook, M. Boota, G. M. Housel, A. McBride, E. C. Kumbur, Y. Gogotsi, Effect of oxidation of carbon material on suspension electrodes for flow electrode capacitive deionization, Environmental Science and Technology 49 (5) (2015) 3040–3047. doi:10.1021/es5055989.

[46] H. Yoon, H. J. Kim, J. J. Yoo, C. Y. Yoo, J. H. Park, Y. A. Lee, W. K. Cho, Y. K. Han, D. H. Kim, Pseudocapacitive slurry electrodes using redox-active quinone for high-performance flow capacitors: An atomic-level understanding of pore texture and capacitance enhancement, Journal of Materials Chemistry A 3 (46) (2015) 23323–23332. doi:10.1039/c5ta05403f.

[47] S. Fletcher, V. J. Black, I. Kirkpatrick, A universal equivalent circuit for carbon-based supercapacitors, Journal of Solid State Electrochemistry 18 (5) (2014) 1377–1387. doi:10.1007/s10008-013-2328-4.

[48] C. Lei, F. Markoulidis, Z. Ashitaka, C. Lekakou, Electrochimica Acta Reduction of porous carbon / Al contact resistance for an electric double-layer capacitor (EDLC) 92 (2013) 183–187.

[49] S. Dsoke, X. Tian, C. Täubert, S. Schlüter, M. Wohlfahrt-Mehrens, Strategies to reduce the resistance sources on Electrochemical Double Layer Capacitor electrodes, Journal of Power Sources 238 (2013) 422–429. doi:10.1016/j.jpowsour.2013.04.031.

[50] E. Barsoukov, J. R. Macdonald, Impedance Spectroscopy: Theory, Experiment, and Applications, 2005.

[51] M. E. Orazem, B. Tribollet, Electrochemical impedance spectroscopy, vol. 48 Edition, John Wiley & Sons, 2011.

[52] R. Kötz, M. Carlen, Principles and applications of electrochemical capacitors, Electrochim. Acta 45 (15-16) (2000) 2483–2498. arXiv:arXiv:1011.1669v3, doi:DOI: 10.1016/S0013-4686(00)00354-6.

[53] R. de Levie, On porous electrodes in electrolyte solutions, Electrochimica Acta 8 (10) (1963) 751–780. doi:10.1016/0013-4686(63)80042-0.
URL http://linkinghub.elsevier.com/retrieve/pii/0013468663800420

[54] R. De Levie, The influence of surface roughness of solid electrodes on electrochemical measurements, Electrochimica Acta 10 (2) (1965) 113–130. doi:10.1016/0013-4686(65)87012-8.